Preparation of an *O*-[2-(methacryloyloxy)-ethylcarbamoyl]-10,11-dihydroquinidine-silica hybrid monolithic column for the enantioseparation of amino acids by nano-liquid chromatography

Dongsheng Xu [a,b,c], Elena Sánchez-López [c,d], Qiqin Wang [a,b], Zhengjin Jiang [a,b, *], María Luisa Marina [c,d, *]

[a] *Institute of Pharmaceutical Analysis, College of Pharmacy, Jinan University, Guangzhou 510632, China.*

[b] *Department of Pharmacy and Guangdong Province Key Laboratory of Pharmacodynamic Constituents of Traditional Chinese Medicine & New Drug Research, Jinan University, Guangzhou 510632, China.*

[c] *Departamento de Química Analítica, Química Física e Ingeniería Química, Universidad de Alcalá, Ctra. Madrid-Barcelona Km. 33.600, 28871 Alcalá de Henares (Madrid), Spain.*

[d] *Instituto de Investigación Química "Andrés M. del Río" (IQAR), Universidad de Alcalá, Ctra. Madrid-Barcelona Km. 33.600, 28871 Alcalá de Henares (Madrid), Spain.*

[*] Corresponding authors. Tel: +34 91 8854935

[*] Corresponding authors. Tel: +86 2085223604

E-mail: mluisa.marina@uah.es (M. L. Marina), jzjjackson@hotmail.com (Z. J. Jiang)

Abstract: An *O*-[2-(methacryloyloxy)-ethylcarbamoyl]-10,11-dihydroquinidine (MQD)-silica hybrid monolithic column was prepared by a facile "one-step" strategy within a 100 μm I.D. capillary. The influence of the methanol, ethylene glycol and water volume ratio, reaction temperature and time, cetyltrimethylammonium bromide and MQD monomers content and volume ratio of tetramethoxysilane and vinyltrimethoxysilane was investigated to obtain a satisfactory morphology of monolithic columns. The optimized MQD-silica hybrid monolithic column was evaluated in terms of permeability, stability, efficiency, reproducibility, and was characterized by scanning electron microscopy and nano-liquid chromatography. Among the 52 N-derivatized protein and non-protein amino acids, a total of 44 analytes could be baseline enantioseparated using the optimized conditions in either reversed phase mode (RPM) or polar organic phase mode (POM). The results showed that POM (ACN/MeOH/HAc/TEA (60/40/0.055/0.005, v/v/v/v)) offered better performance than RPM (ACN/10 mM ammonium acetate (70/30, v/v) (apparent pH=5.3)) in terms of enantioresolution and efficiency with shorter analysis times.

Keywords: Quinidine, Enantioseparation, Hybrid monolith, Nano-Liquid Chromatography

52 **1. Introduction**

53 Chiral analysis is a relevant topic in separation sciences due to its profound impact
54 in different fields such as pharmaceutical, agrochemical and food industry. Nowadays,
55 many possibilities are available to carry out a successful chiral separation, in which
56 micro-separative techniques play a vital role due to the advantages derived from their
57 inherent low dimensions. Among the different miniaturized strategies to achieve chiral
58 separations, the use of chiral columns in nano-liquid chromatography (nano-LC) or
59 capillary electrochromatography (CEC) has attracted much interest. Specifically,
60 monolithic stationary phases functionalized with quinidine or quinine have been used
61 in enantioseparation by these two techniques [1-3] and have demonstrated to offer an
62 excellent chiral separation ability for various kinds of acidic compounds such as amino
63 acids [4-5], small peptides [6], or profens [7-8]. Recently, several quinine and
64 quinidine-based monolithic columns have been developed by Lämmerhofer *et al.*, such
65 as organic polymer-based monoliths, *O*-[2-(methacryloyloxy)-ethylcarbamoyl]-10,11-
66 dihydroquinidine-*co*-2-hydroxyethyl methacrylate-*co*-ethylene dimethacrylate [1, 9-
67 10], *O*-9-(*tert*-butylcarbamoyl)-11-[2-(methacryloyloxy)ethylthio]-10,11-
68 dihydroquinine-*co*-2-hydroxyethyl methacrylate-*co*-ethylene dimethacrylate [2], *O*-9-
69 (*tert*-butylcarbamoyl)-quinine-*co*- glycidylmethacrylate-*co*-ethylene dimethacrylate
70 [11], *O*-9-(*tert*-butylcarbamoyl)-quinine-*co*-3-mercaptopropyl methylsiloxane-*co*-
71 glycidylmethacrylate-*co*-ethylene dimethacrylate [12-13]; and silica-based monoliths,
72 *O*-9-(tert-butylcarbamoyl)-11-[2-(methacryloyloxy)ethylthio]-10,11-dihydroquinine
73 [14] and *O*-9-(tert-butylcarbamoyl)-quinine [15]. The aim of those works was mainly
74 to describe the preparation strategy for those monolithic columns and their ability to
75 enantioseparate several N-derivatized amino acids and 2-aryloxypropionic acids. Wang
76 and co-workers developed several organic polymer-based quinidine monoliths, namely
77 *O*-[2-(methacryloyloxy)-ethylcarbamoyl]-10,11-dihydroquinidine-*co*-2-hydroxyethyl
78 methacrylate-*co*-ethylene dimethacrylate (poly(MQD-*co*-HEMA-*co*-EDMA)) [4, 16],
79 and *O*-[2-(methacryloyloxy)-ethylcarbamoyl]-10,11-dihydroquinidine-*co*-ethylene
80 dimethacrylate (poly (MQD-*co*-EDMA)) [5], and *O*-9-(*tert*-butylcarbamoyl)-11-[2-
81 (methacryloyloxy)ethylthio]-10,11-dihydroquinidine (poly (MBQD-*co*-HEMA-
82 EDMS)) [3]. On the optimized monolithic columns, 44 N-derivatized amino acids and
83 53 small peptides were enantioseparated [4, 6]. So far, the major category of quinidine
84 functionalized monoliths is silica- or polymer-based. However, to the best of our
85 knowledge, a quinidine functionalized organic-inorganic hybrid monolithic column has

never been reported before.

Over the years, organic-inorganic hybrid monolithic columns have been developed because of their excellent permeability, higher pH stability, high surface, and superior performance [17-19]. Compared with the polymer-based and silica-based monoliths, the less shrinkage for organic-silica hybrid monolith has received increasing attention [20-22]. Hence, Tran *et al.* [7, 8] developed quinine-silica/zirconia and *tert*-butylcarbamoylquinine (*t*BuCQUI)-silica hybrid monolith using polyethylene glycol (PEG), vinyltrimethoxysilane (VTMS) and tetramethoxysilane (TMOS), which influence the phase separation time, hydrolyzation and condensation, respectively. However, only several profens and dinitrobenzoyl (DNB) chloride derivatized amino acids have been enantioseparated on the two hybrid monolithic columns, and the preparation process was time-consuming due to the multi-step temperature regulation used. In addition, several articles reported that reversed phase mode (RPM) and polar organic phase mode (POM) can both be used in enantioseparation [1, 6, 9]. However, to the best of our knowledge, only RPM has been used in the quinine functionalized organic-inorganic hybrid monolithic column.

In this work, an *O*-[2-(methacryloyloxy)-ethylcarbamoyl]-10,11-dihydroquinidine (MQD)-silica hybrid monolithic column was prepared within a 100 μm I.D. capillary through a facile "one-step" strategy. In order to obtain a satisfactory permeability, the methanol (MeOH)/ethylene glycol (EG) (v/v), H_2O/ammonium hydroxide ($NH_3 \cdot H_2O$) (v/v), cetyltrimethylammonium bromide (CTAB) (mg), TMOS/VTMS (v/v), monomer (MQD) (mg) in the pre-polymerizable mixture and the reaction temperature and time were optimized in order to obtain the best column efficiency and enantioresolution for a set of N-derivatized amino acids. The mobile phase composition was evaluated on the optimized MQD-silica hybrid monolithic column under the RPM and POM conditions, and a total of 52 N-derivatized protein and non-protein amino acids were enantioseparated under both mobile phase modes. Finally, the two different mobile phase modes were compared in terms of enantioselectivity (α), analysis time, enantioresolution (R_s) and column efficiency (N).

2. Materials and methods

2.1. Reagents and solvents

10,11-dihydroquinidine, 2,2'-azobisisobutyronitrile (AIBN), 3-(trimethoxysilyl)-propylmethacrylate (γ-MAPS), 2-isocyanatoethyl methacrylate (ICNEML), VTMS,

CTAB, TMOS and EG were acquired from Aladdin Chemicals (Shanghai, China). MeOH, tetrahydrofuran (THF), chloroform ($CHCl_3$), acetonitrile (ACN) and acetic acid (HAc) were acquired from Scharlau Chemie (Barcelona, Spain). Triethylamine (TEA) and 9-fluorenylmethoxycarbonyl (FMOC) chloride were obtained from Fluka (Buchs, Switzerland). $NH_3 \cdot H_2O$, boric acid (H_3BO_3) and pentane were from Sigma (St. Louis, Missouri, USA), and ammonium acetate was from Merck (Darmstadt, Germany). 3,5-dinitrobenzoyl (3,5-DNB) chloride, *p*-nitrobenzoyl (*p*-NB) chloride, 3,5-dimethoxybenzoyl chloride (3,5-DMB), 3,5-dichlorobenzoyl chloride (3,5-DCIB), m-chlorobenzoyl chloride (m-CIB), *p*-chlorobenzoyl chloride (*p*-CIB), benzoyl chloride (B) and propylene oxide were purchased from Tokyo Chemical Industry Co., Ltd. (Tokyo, Japan). DL-arginine, DL-histidine, DL-lysine, DL-serine, DL-threonine, DL-asparagine, DL-glutamine, DL-cysteine, DL-proline, DL-alanine, DL-valine, DL-leucine, DL-methionine, DL-phenylalanine, DL-tyrosine, DL-tryptophan, DL-ornithine and DL-citrulline standards were obtained from Fluka (Buchs, Switzerland), while DL-isoleucine, DL-aspartic acid, DL-glutamic acid, DL-norvaline, DL-norleucine, DL-dioxyphenylalanine, DL-pyroglutamic acid and DL-methionine sulfone were obtained from Sigma (St. Louis, Missouri, USA). All the N-derivatized amino acids were synthesized as previously described [4].

Fused-silica capillaries (375 μm O.D. × 100 μm I.D.) were obtained from Ruifeng Chromatography Ltd. (Hebei, China). Distilled water was purified using a Milli-Q water system from Millipore (Massachusetts, USA). Reversed phase mobile phases were prepared by mixing ACN and ammonium acetate buffer solvents and adjusting the apparent pH to the desired value using HAc. Polar organic mobile phases were set up by mixing the desired ratio of ACN and MeOH, and then adding various amounts of HAc and TEA. All mobile phases were subjected to filtration through a 0.22 μm membrane and sonicated prior use.

2.2. Instrumentation

The molecular mass of the MQD monomer was determined on an AB Sciex QTrap 4500 mass spectrometer (California, USA). A Jinghong DKS22 water bath (Shanghai, China) was used for thermally initiated copolymerization. Scanning electron microscopy (SEM) experiments were performed on a Zeiss Gemini ultra-55 SEM (Deutschland, Germany) at an acceleration voltage of 5 kV. All nano-LC experiments were conducted on a laboratory self-assembled instrument. The system consisted of a

154 Shimadzu LC-20AD pump (Kyoto, Japan), a Linear Instruments UVIS-200 detector
155 (California, USA), and a Valco four-port injection valve with a 20 nL internal loop
156 (Houston, USA). In order to reduce the flow rate, a stainless-steel tee (Cheminert, Valco
157 Instruments Houston, Texas, USA) with a flow split capillary (150 mm × 25 μm I.D.)
158 was employed before the injection valve. Data acquisition and handling were performed
159 using the software Chromatostation N200 (Zhejiang University, China). All
160 chromatograms were converted to a text file and then redrawn using Microcal Origin
161 8.5. The pH values of buffer solutions were measured by a 744 pH meter (Herisau,
162 Switzerland).
163

164 **2.3. Preparation of the MQD-silica hybrid monolithic column**

165 At the beginning, the fused-silica capillary inner wall was modified using γ-
166 MAPS/MeOH (50/50, v/v), in order to provide the anchoring sites for the bulk polymer
167 [3], and the chiral functional monomer MQD was synthesized according to a previously
168 reported method [1, 4], the MS spectrum (ESI+) of the purified product is depicted in
169 **Fig. S1** where an ion at *m/z* 482.2, i.e. the $[M+H]^+$ ion from the functional MQD
170 monomer, is observed.

171 The schematic representation of the preparation of the MQD-silica hybrid
172 monolithic column is illustrated in **Fig. 1**. The pre-polymerizable mixture for preparing
173 the MQD-silica hybrid monolithic column was obtained by mixing the MQD (6.0 mg),
174 MeOH (100 μL), EG (30 μL), CTAB (1.6 mg), H_2O (30 μL), $NH_3 \cdot H_2O$ (0.02 M, 30 μL),
175 TMOS (60 μL), VTMS (80 μL), and AIBN (1 mg) in a 2-mL vial. After sonicating for
176 5 min at room temperature, a homogeneous solution was obtained and was then
177 introduced into the 30 cm pretreated capillary. Then, both ends of the capillaries were
178 sealed with GC septa and submerged into the water bath (40 ºC) for 12 h and followed
179 by another 12 h at 60 ºC. The unreacted CTAB and other residuals were removed by
180 flushing the column with methanol. The obtained monolith column was cut to 15 cm
181 for nano-LC analysis. A 2-5 mm length of the monolith column was used for SEM
182 analysis (**Fig. S2**).
183

184 **3. Results and discussion**

185 **3.1. Preparation and characterization of the MQD-silica hybrid monolithic**
186 **column**

187 **3.1.1. Preparation of the MQD-silica hybrid monolithic column**

188 Previous research has proved that the physicochemical and chromatographic
189 properties of the hybrid monolithic column can be controlled by changing the pre-
190 polymerizable mixture [18]. In order to obtain a hybrid monolithic column with a good
191 permeability, the solvent combination (MeOH, EG, H_2O and $NH_3 \cdot H_2O$), the content of
192 the CTAB, MQD monomer, the ratio of TMOS/VTMS (v/v) and the reaction time and
193 temperature were investigated under the microscope, as shown in **Table 1**.

194 First, the combination of different solvents (H_2O, MeOH, ethanol, DMF, DMSO,
195 THF, benzyl alcohol, EG, ethyl acetate, 1,4-butanediol and 1-propanol) was tested.
196 Among the different solvents evaluated, a ternary system containing H_2O, MeOH and
197 EG was selected because of its good solubility for MQD. Then, the influence of the
198 MeOH/EG ratio (v/v) and the content of H_2O was studied by varying them from 95/35
199 (column **C1**) to 105/25 (column **C3**), and from 25 μL (column **C4**) to 35 μL (column
200 **C5**), respectively. As can be observed in the microscope images from **Table 1**, the
201 column **C2** prepared with MeOH/EG/H_2O/$NH_3 \cdot H_2O$ (100/30/30/30, v/v/v/v) exhibited
202 a very good morphology in the microscope images when compared to columns **C1**
203 (slack morphology), **C3** (semitransparent morphology), **C4** (transparent morphology)
204 and **C5** (slack morphology), therefore, it was selected for the following studies.

205 The CTAB content has proved to have a strong impact on the hybrid column
206 morphology [18]. Different weight fractions of CTAB were assayed: 1.2 mg (column
207 **C6**), 1.6 mg (column **C2**) and 2.0 mg (column **C7**). The column **C6** showed a
208 semitransparent morphology because of the low content of CTAB, but the column **C7**
209 was slack. Because CTAB acts as a supramolecular template in the reaction process for
210 hybrid monolithic column, high amounts of CTAB in the pre-polymerizable mixture
211 results in a slack morphology for the monolith. Therefore, an amount of 1.6 mg of
212 CTAB (column **C2**) was selected for the next studies.

213 In order to get a homogeneous solution which can be introduced into the capillary,
214 the reaction of hydrolysis and polycondensation necessary to prepare the hybrid
215 monolithic column was adjusted based on the ratio of TMOS/VTMS and the content of
216 MQD. Different TMOS/VTMS ratios (μL, v/v) were tested from 55:85 (column **C8**) to
217 65:75 (column **C9**) and the content of MQD was tested from 4.0 mg (**C10**) to 8.0 mg
218 (**C11**). All the morphologies obtained can be seen in **Table 1**. When decreasing the
219 content of VTMS and MQD, while other conditions were kept constant, the morphology
220 image of the monolithic column became slacker. Finally, a TMOS/VTMS ratio of 60:80

(μL, v/v) and MQD 6.0 mg (column **C2**) was chosen for the following experiment because it was a transparent and homogeneous solution which was easier to introduce into the capillary.

Another aspect to take into account is the reaction temperature and time as they affect the morphology and permeability of the monolithic column. Three different conditions were tested: 40 ℃ during 12 h followed by 60 ℃ during 12 h (column **C2**), 40 ℃ for 24 h (column **C12**) and 60 ℃ during 24 h (column **C13**). The microscope images of the columns prepared under the different temperatures and times are shown in **Table 1**. Column **C2** was selected because of the monolithic column exhibited a good morphology image.

Based on these optimization experiments, the pre-polymerizable mixture consisting on MeOH (100 μL), EG (30 μL), H_2O (30 μL), $NH_3 \cdot H_2O$ (0.02 M, 30 μL), TMOS (60 μL), VTMS (80 μL), CTAB (1.6 mg), MQD (6.0 mg) and AIBN (1.0 mg) was chosen, conducting the reaction at 40 °C for 12 h followed by 60 °C for 12 h. As shown in **Fig. S2**, the morphology of the MQD-silica hybrid monolithic column (column **C2**) was evaluated by SEM, and the SEM images indicated that the column **C2** had the morphology of a continuous skeleton and large through-pores, and the monolithic rod was tightly anchored on the inner wall of the capillary column.

3.1.2. Physicochemical evaluation of the MQD-silica hybrid monolithic column

The permeability (K) of the monolithic column can be calculated using the following equation [23,24]:

$$K = \frac{u\eta L}{\Delta P}$$

being u the linear velocity of the mobile phase, L the length of the column, ΔP the pressure drop across the column, and η the dynamic viscosity of the eluent. Toluene (ACN or MeOH as mobile phase) and thiourea (ACN/H_2O (50/50, v/v) as mobile phase) were selected as the dead time markers. As can be seen in **Table S1**, the calculated K values for the chosen column (column **C2**) were 2.95×10^{-14}, 2.93×10^{-14} and 2.47×10^{-14} m^2 when using ACN, MeOH and ACN/H_2O (50/50, v/v) as the mobile phases, respectively. As can be seen in **Fig. S3**, the mechanical stability showed satisfactory linearity between the linear velocity and the backpressure, in the range of 5-100 bar, the R^2 values for ACN, MeOH and H_2O/ACN (50/50, v/v) were 0.9996, 0.9997, 0.9988, respectively. Overall, the results indicated good permeability and mechanical stability

254 for the optimized MQD-silica hybrid monolithic column in the solvents with different
255 polarities.
256
257 **3.1.3. Reproducibility of the MQD-silica hybrid monolithic column**
258 The reproducibility of the MQD-silica hybrid monolithic column was evaluated
259 through the RSD values for retention factors (k_1, k_2), α and R_s of the N-derivatized
260 racemic *p*-NB-leucine using a mixture of ACN/10 mM ammonium acetate (70/30, v/v)
261 (apparent pH 5.3) as mobile phase (see **Table S2**). The run-to-run RSDs (n=6) for k_1
262 and k_2 were 1.81% and 1.24%, while the column-to-column RSDs (n=5) for the
263 retention factors were 2.53% and 3.05%, respectively. The batch-to-batch repeatability
264 (n=3) for k_1 and k_2 was also adequate with RSDs values of 4.29% and 3.59%,
265 respectively, in addition to day-to-day repeatability (n=3) which were 1.73% and 1.69%,
266 respectively. RSD values of α and R_s were also satisfactory: ≤ 4.04. These data clearly
267 indicated that the MQD-silica hybrid monolithic column has a satisfactory
268 reproducibility for enantioseparation in nano-LC.
269
270 **3.2. Effects of the mobile phase composition**
271 **3.2.1. Reversed phase mode**
272 As reported in previous studies [4], two N-derivatized amino acids (*p*-NB-leucine
273 (see **Figure 2**), 3,5-DMB-leucine (see **Table S3**)) were selected as test analytes, and the
274 k, α and R_s were used to evaluate the MQD-silica hybrid monolithic column, in the
275 RPM. In order to obtain satisfactory enantioseparation conditions, the concentration of
276 the organic solvent, apparent pH and buffer concentration in the mobile phase were
277 optimized.
278 The effect of the apparent pH of the mobile phase was evaluated from 4.3 to 6.3,
279 while the mobile phase composition was kept constant (ACN/5 mM ammonium acetate
280 (80/20, v/v)). As shown in **Figure 2a and b**, the k_1 increased with increasing the
281 apparent pH. On the other hand, R_s improved with increasing the apparent pH from 4.3
282 to 5.3, and then levelled off from 5.3 to 6.3. These results are also in agreement with
283 previous studies [4]. A high apparent pH of the mobile phase would lead to a higher
284 negative charge of the two N-derivatized amino acids (*p*-NB-leucine and 3,5-DMB-
285 leucine), resulting in a stronger electrostatic interaction with the positively charged
286 quinidine chiral stationary phase. Hence, an apparent pH of 5.3 was chosen for the
287 following experiments.

288 The influence of the ACN concentration in the mobile phase on the k_1 and R_s also
289 evaluated. As shown in **Figure 2c**, both k_1 and R_s decreased when increasing the ACN
290 concentration from 60 to 90% (v/v). This is due to the fact that a higher ACN
291 concentration would cause a weaker hydrophobic interaction between the CSP and the
292 tested enantiomers. Thus, 70% (v/v) ACN was selected for the following experiments
293 as a compromise between the analysis time and enantioresolution.
294 The concentration of the ammonium acetate buffer was also studied from 1 to 30
295 mM. As shown in **Figure 2d**, when increasing the buffer concentration in the mobile
296 phase, both k_1 and R_s decreased. Moreover, it was found that when the concentration of
297 buffer was low (1 mM), R_s were adequate for the two test analytes, while their analysis
298 times were rather long (>60 min). Finally, 10 mM ammonium acetate buffer was
299 selected as the optimum mobile phase modifier.
300 Under the optimal RPM conditions which consist of ACN/10 mM ammonium
301 acetate (70/30, v/v) (apparent pH=5.3), 52 N-derivatized amino acids were tested. As
302 shown in **Table 2**, 42 out of 52 were baseline enantioseparated (R_s > 1.5) on the
303 monolithic column. However, most of N-derivatized FMOC amino acids were not
304 baseline enantioseparated, except the FMOC-isoleucine and FMOC-valine (R_s were
305 1.55 and 1.71, respectively). **Fig. 3** displays the enantioseparation for *p*-NB-leucine, *p*-
306 CIB-Alanine, *p*-CIB-Methionine, 3,5-DMB-Leucine, 3,5-DCIB-Alanine and *p*-NB-
307 Methionine.
308
309 **3.2.2. Polar organic phase mode**
310 The second mode to be assayed was the POM. According to previous studies [6],
311 N-derivatized amino acids can be enantioresolved in POM, specifically in a mobile
312 phase consisting of ACN/MeOH and HAc/TEA. In this study, B-leucine (see **Figure 4**)
313 and 3,5-DCIB-leucine (see **Table S4**) were selected as the test analytes. The ratio of
314 MeOH/ACN, HAc/TEA and the total concentration of HAc and TEA were optimized
315 as in previous reports [25-27].
316 The influence of the MeOH/ACN ratio on the k_1 and R_s for the two test analytes
317 was evaluated from 60/40 (%, v/v) to 20/80 (%, v/v), while the total concentration of
318 TEA and HAc was kept constant. As shown in **Figure 4a and b**, the k_1 increased
319 gradually with decreasing the MeOH concentration from 60 to 20% (v/v). However,
320 the R_s increased when increasing the content of MeOH from 20 to 40% (v/v), then
321 decreased when further increasing the content to 60% (v/v). Hence, 40:60 (MeOH/ACN,

322 v/v) was selected as the optimum mobile phase for the following experiments.

323 After, the effect of the total concentration of HAc+TEA was evaluated from 0.015
324 to 0.48% (v/v), while the ratio of HAc/TEA (5/1, v/v) was kept constant (see **Figure**
325 **4c**). The N_1 increased when the total concentration of HAc+TEA increased from 0.015
326 to 0.48% (v/v). The highest total concentration of HAc+TEA would lead to higher
327 efficiency and shorter analysis time, because of the weaker interaction between the
328 enantiomers and the CSP when increasing the concentration of the competing acetate
329 anion in the solvent. On the other hand, the R_s increased when increasing the
330 concentration of HAc+TEA from 0.015 to 0.06% (v/v), then it decreased when the
331 concentration of HAc+TEA increased up to 0.48% (v/v). Thus, a total concentration of
332 0.06% (v/v) for HAc+TEA was used for further experiments because it enabled to
333 obtain the highest enantioresolution.

334 Finally, the HAc/TEA ratio was investigated. As can be seen in **Figure 4d**, the R_s
335 and N_1 of B-leucine increased when increasing the ratio of HAc/TEA from 3:1 (%, v/v)
336 to 5:1 (%, v/v), then remained almost constant from 5:1 (%, v/v) to 29:1 (%, v/v). In
337 the case of 3,5-DCIB-Leucine (see **Table S4**) the R_s kept increasing and remained
338 almost constant at 11:1 (%, v/v) and 29:1 (%, v/v). As a compromise, a HAc/TEA ratio
339 of 11:1 (%, v/v) was selected.

340 Under the optimal POM conditions, this is, MeOH/ACN (40/60, v/v), 0.055%
341 (v/v) HAc and 0.005% (v/v) TEA (i.e., a 11:1 HAc/TEA (%, v/v) ratio), 52 N-
342 derivatized amino acids were tested. It is important to note that the peaks of 3,5-DCIB-
343 methionine, 3,5-DMB-threonine, *m*-CIB-threonine and B-threonine were deteriorated
344 when using the optimal POM conditions (see **Fig. S4**), thus, mobile phase conditions
345 had to be slightly modified. As can be seen in **Table 3**, also 44 out of 52 were finally
346 baseline enantioseparated ($R_s > 1.5$) on the monolithic column using POM conditions.
347 Same as in RPM, most of FMOC-derivatized amino acids also can not be baseline
348 enantioresolved. The enantioseparations for *p*-NB-leucine, *p*-CIB-alanine, *p*-CIB-
349 methionine, 3,5-DMB-leucine, 3,5-DCIB-alanine and *p*-NB-methionine under POM
350 conditions were displayed in **Fig. 5**.

351

352 **3.3. Comparison of the enantioseparation of *N*-derivatized amino acids under**
353 **POM and RPM conditions**

354 In order to further investigate the enantioseparation ability of the MQD-silica
355 hybrid monolithic column for the 52 N-derivatized amino acids, the results obtained

356 under RPM and POM conditions were compared in terms of the α, R_s, N_1 and analysis
357 time.

358 A total of 44 N-derivatized amino acids could be enantioseparated in both RPM
359 and POM with similar α values (Fig. 6). Comparing the α values for all the amino acids
360 in the same mode, the higher electrophilic character of the N-protecting groups would
361 lead to a higher enantioselectivity, following this trend: 3,5-DNB-leucine (α = 4.22)>
362 3,5-DCIB-leucine (α = 2.62)> 3,5-DMB-leucine (α = 1.91)> *m*-CIB-leucine (α = 1.80)>
363 *p*-NB-leucine (α = 1.73)> *p*-CIB-leucine (α=1.58)> B-leucine (α=1.33) (in the case of
364 RPM; similar trend was found for POM). Regarding the enantioresolution and column
365 efficiency (Fig. 7), these values were higher in POM than in RPM. Unfortunately, most
366 of FMOC-derivatized amino acids were not baseline enantioseparated in any of the two
367 modes (except the FMOC-isoleucine and FMOC-valine which could be baseline
368 enantioseparated in RPM), as earlier commented. Regarding the analysis time values,
369 they were shorter in POM when compared to RPM for all the N-derivatized amino acids
370 tested (Fig. 6).

371 Overall, the POM offered better performance than RPM for the N-derivatized
372 amino acids herein tested in terms of the enantioresolution, efficiency and analysis time.
373

374 **4. Conclusions**

375 This study shows a straightforward "one-step" strategy to prepare a MQD-silica
376 hybrid monolithic column within a 100 µm I.D. capillary. Under the optimal preparation
377 conditions, the resulting monolithic column exhibited good permeability, mechanical
378 stability, and reproducibility. After the optimization of the both RPM and POM
379 chromatographic conditions, a total of 52 N-derivatized amino acids were
380 enantioseparated in nano-LC, and baseline enantioseparation was observed for 44 of
381 them in both modes. Most of FMOC-derivatized amino acids were not baseline
382 separated under both chromatographic modes although chiral discrimination was
383 observed for all of them. When comparing RPM and POM chromatographic modes, the
384 POM offered better performance than RPM in terms of column efficiency and
385 enantioresolution with shorter analysis time.
386

387 **5. Acknowledgements**

388 M. L. Marina and E. Sánchez-López thank the Ministry of Economy and

Competitiveness (Spain) for research projects CTQ2013-48740-P and CTQ2016-76368-P. D. Xu and E. Sánchez-López thank the Comunidad of Madrid and European funding from FEDER program for their contracts (AVANSECAL-CM program, ref. S2013/ABI-3028).

393 **References**

394 [1] M. Lämmerhofer, E.C. Peters, C. Yu, F. Svec, J.M.J. Fréchet, Chiral monolithic
395 columns for enantioselective capillary electrochromatography prepared by
396 copolymerization of a monomer with quinidine functionality. 1. Optimization of
397 polymerization conditions, porous properties, and chemistry of the stationary
398 phase, Anal. Chem. 72 (2000) 4614-4622.
399 [2] M. Lämmerhofer, E. Tobler, E. Zarbl, W. Lindner, F. Svec, J.M.J. Fréchet,
400 Macroporous monolithic chiral stationary phases for capillary
401 electrochromatography: New chiral monomer derived from cinchona alkaloid with
402 enhanced enantioselectivity, Electrophoresis 24 (2003) 2986-2999.
403 [3] Q.Q. Wang, P.J. Zhu, M. Ruan, H.H. Wu, K. Peng, H. Han, G. W. Somsen, J.
404 Crommen, Z.J. Jiang, Chiral separation of acidic compounds using an *O*-9-(*tert*-
405 butylcarbamoyl) quinidine functionalized monolith in micro-liquid
406 chromatography, J. Chromatogr. A 1444 (2016) 64-73.
407 [4] Q.Q. Wang, J. Feng, H. Han, P.J. Zhu, H.H. Wu, M.L. Marina, J. Crommen, Z.J.
408 Jiang, Enantioseparation of N-derivatized amino acids by micro-liquid
409 chromatography using carbamoylated quinidine functionalized monolithic
410 stationary phase, J. Chromatogr. A 1363 (2014) 207-215.
411 [5] H.H. Wu, Q.Q. Wang, M. Ruan, K. Peng, P.J. Zhu, J. Crommen, H. Hai, Z.J. Jiang,
412 Enantioseparation of N-derivatized amino acids by micro-liquid
413 chromatography/laser induced fluorescence detection using quinidine-based
414 monolithic columns, J. Pharm. Biomed. Anal. 121 (2016) 244-252.
415 [6] Q.Q. Wang, E. Sánchez-López, H. Han, H.H. Wu, P.J. Zhu, J. Crommen, M.L.
416 Marina, Z.J. Jiang, Separation of N-derivatized di- and tri-peptide stereoisomers
417 by micro-liquid chromatography using a quinidine-based monolithic column -
418 Analysis of l-carnosine in dietary supplements, J. Chromatogr. A 1428 (2016) 176-
419 184.
420 [7] L.N. Tran, J.H. Park, Enantiomer separation of acidic chiral compounds on a
421 quinine-silica/zirconia hybrid monolith by capillary electrochromatography, J.
422 Chromatogr. A 1396 (2015) 140-147.

423 [8] L.N. Tran, J.A. Jeong, J.H. Park, Enantiomer separation of acidic chiral compounds
424 on a *tert*-butylcarbamoylquinine-silica hybrid monolith by capillary
425 electrochromatography, Bull. Korean Chem. Soc. 37 (2016) 1050-1056.
426 [9] M. Lämmerhofer, F. Svec, J.M.J. Fréchet, Chiral monolithic columns for
427 enantioselective capillary electrochromatography prepared by copolymerization
428 of a monomer with quinidine functionality. 2. Effect of chromatographic
429 conditions on the chiral separations, Anal. Chem. 72 (2000) 4623-4628.
430 [10] M. Lämmerhofer, F. Svec, J.M.J. Fréchet, W. Lindner, Monolithic stationary
431 phases for enantioselective capillary electrochromatography, J. Micro. Sep. 12
432 (2000) 597-602.
433 [11] B. Preinerstorfer, W. Bicker, W. Lindner, M. Lämmerhofer, Development of
434 reactive thiol-modified monolithic capillaries and in-column surface
435 functionalization by radical addition of a chromatographic ligand for capillary
436 electrochromatography, J. Chromatogr. A 1044 (2004) 187-199.
437 [12] E.J. Carrasco-Correa, G. Ramis-Ramos, J.M. Herrero-Martínez, M. Lämmerhofer,
438 Polymethacrylate monoliths with immobilized poly-3-mercaptopropyl
439 methylsiloxane film for high-coverage surface functionalization by thiol-ene click
440 reaction, J. Chromatogr. A 1367 (2014) 123-130.
441 [13] M. Wolter, M. Lämmerhofer, In-situ functionalized monolithic polysiloxane
442 polymethacrylate composite materials from polythiol-ene double click reaction in
443 capillary column format for enantioselective nano-high-performance liquid
444 chromatography, J. Chromatogr. A 1497 (2017) 172-179.
445 [14] S. Buchinger, B. Follrich, M. Lämmerhofer, D. Lubda, W. Lindner, Chirally
446 functionalized anion-exchange type silica monolith for enantiomer separation of
447 2-aryloxypropionic acid herbicides by non- aqueous capillary
448 electrochromatography, Electrophoresis 30 (2009) 3804-3813.
449 [15] B. Preinerstorfer, D. Lubda, A. Mucha, P. Kafarski, W. Lindner, M. Lämmerhofer,
450 Stereoselective separations of chiral phosphinic acid pseudodipeptides by CEC
451 using silica monoliths modified with an anion-exchange-type chiral selector,
452 Electrophoresis 27 (2006) 4312-4320.
453 [16] Q.X. Zhang, V. Gil, E. Sánchez-López, M.A. García, Z.J. Jiang, M.L. Marina,

Evaluation of the potential of a quinidine-based monolithic column on the enantiomeric separation of herbicides by nano-liquid chromatography, Microchem. J. 123 (2015) 15-21.

[17] H. Lin, J. Ou, Z. Zhang, J. Dong, M. Wu, H. Zou, Facile preparation of zwitterionic organic-silica hybrid monolithic capillary column with an improved "one-pot" approach for hydrophilic-interaction liquid chromatography (HILIC), Anal. Chem. 84 (2012) 2721-2728.

[18] Z. Zhang, M. Wu, R. Wu, J. Dong, J. Ou, H. Zou, Preparation of perphenylcarbamoylated β-cyclodextrin-silica hybrid monolithic column with "one-pot" approach for enantioseparation by capillary liquid chromatography, Anal. Chem. 83 (2011) 3616-3622.

[19] H. Zhang, J. Ou, Z. Lui, H. Wang, Y. Wei, H. Zou, Preparation of hybrid monolithic columns via "one-pot" photoinitiated thiol-acrylate polymerization for retention-independent performance in capillary liquid chromatography, Anal. Chem. 87 (2015) 8789-8797.

[20] J. Ou, H. Lin, Z. Zhang, G. Huang, J. Dong, H. Zou, Recent advances in preparation and application of hybrid organic-silica monolithic capillary columns, Electrophoresis 34 (2013) 126-140.

[21] D.S. Domingues, I.D. de Souza, M.E.C. Queiroz, Analysis of drugs in plasma samples from schizophrenic patients by column-switching liquid chromatography-tandem mass spectrometry with organic-inorganic hybrid cyanopropyl monolithic column, J. Chromatogr. B 993-994 (2015) 26-35.

[22] H. Zhao, H. Lyu, W. Qin, Z. Xie, Synthesis of boronate-functionalized organic-inorganic hybrid monolithic column for the separation of cis-diol containing compounds at low pH, Electrophoresis 39 (2018) 924-932.

[23] Z.J. Jiang, N.W. Smith, P.D. Ferguson, M.R. Taylor, Hydrophilic interaction chromatography using methacrylate-based monolithic capillary column for the separation of polar analytes, Anal. Chem. 79 (2007) 1243-1250.

[24] J. Lin, S. Liu, J. Lin, X. Lin, Z. Xie, Novel highly hydrophilic methacrylate-based monolithic column with mixed-mode of hydrophilic and strong cation-exchange interactions for pressurized capillary electrochromatography, J. Chromatogr. A 1218 (2011) 4671-4677.

[25] D. Xu, H. Shao, R. Luo, Q. Wang, E. Sánchez-López, S. Fanali, M.L. Marina, Z. Jiang, A facile and efficient single-step approach for the fabrication of vancomycin functionalized polymer-based monolith as chiral stationary phase for nano-liquid chromatography, J. Chromatogr. A 1557 (2018) 43-50.

[26] M.L. Hsieh, L.K. Chau, Y.S. Hon, Single-step approach for fabrication of vancomycin-bonded silica monolith as chiral stationary phase, J. Chromatogr. A 1358 (2014) 208-216.

[27] X.L. Dong, J. Dong, J.J. Ou, Y. Zhu, H.F. Zou, Preparation and evaluation of a vancomycin immobilized silica monolith as chiral stationary phase for CEC, Electrophoresis 28 (2007) 2606-2612.

497 **Figure captions:**

498 **Fig. 1**. Schematic representation of the preparation of the MQD-silica hybrid monolith.

499 **Fig. 2**. Effect of the apparent pH values on (a) retention factor and enantioselectivity;
500 (b) enantioseparation and column efficiency; effect of the (c) content of ACN and (d)
501 concentration of the buffer for *p*-NB-leucine on the retention factor and
502 enantioresolution, in the reversed phase mode. Experimental conditions: (a) and (b)
503 ACN/5 mM ammonium acetate (80/20, v/v) (at the desired apparent pH values); (c)
504 ACN/5 mM ammonium acetate (at the desired ratio of ACN and buffer, v/v) (apparent
505 pH=5.3); (d) ACN/ammonium acetate (at the desired concentration of the buffer)
506 (70/30, v/v) (apparent pH=5.3). Column dimensions: 15 cm × 100 μm I.D.; UV
507 detection wavelength: 254 nm; flow rate: 10 μL/min; injection volume: 20 nL.

508 **Fig. 3**. Enantioseparation of some N-derivatized amino acids in the reversed phase
509 mode. Mobile phase: ACN/10 mM ammonium acetate (70/30, v/v) (apparent pH=5.3);
510 Other experimental conditions are the same as in **Figure 2**.

511 **Fig. 4**. Effect of the MeOH content on (a) retention factor and enantioselectivity; (b)
512 enantioseparation and column efficiency; effect of the (c) concentration and (d) ratio of
513 the HAc/TEA for B-leucine retention factor and enantioresolution in the polar organic
514 phase mode. Experimental conditions: (a) and (b) MeOH/ACN/HAc/TEA (at the
515 desired ratio of MeOH and ACN/0.2/0.04, v/v/v/v); (c) MeOH/ACN/HAc/TEA
516 (40/60/at the desired content of HAc and TEA, v/v/v/v); (d) MeOH/ACN/HAc/TEA
517 (40/60/at the desired ratio of HAc and TEA, v/v/v/v). Column dimensions: 15 cm × 100
518 μm I.D.; UV detection wavelength: 254 nm; flow rate: 10 μL/min; injection volume:
519 20 nL.

520 **Fig. 5**. Enantioseparation of some N-derivatized amino acids in the polar organic phase
521 mode. Mobile phase: ACN/MeOH/HAc/TEA (60/40/0.055/0.005, v/v/v/v); Other
522 experimental conditions are the same as in **Figure 4**.

523 **Fig. 6**. Comparison of the enantioselectivity and analysis time (time of the second
524 enantiomer) under the reversed phase mode and polar organic phase mode.
525 Experimental conditions for reversed phase mode and polar organic mode as in **Figure**
526 **2** and **Table 5**, respectively.

527 **Fig. 7**. Comparison of the enantioresolution and efficiency under the reversed phase
528 mode and the polar organic phase mode. Experimental conditions for reversed phase
529 mode and polar organic mode as in **Figure 2** and **Table 5**, respectively.

530 **Tables captions:**

531 **Table 1**. Effect of the preparation parameters for the MQD-silica hybrid monolithic
532 columns.

533 **Table 2**. Enantioseparation of N-derivatized amino acids in the reversed phase mode.
534 Experimental conditions are the same as in **Figure 3**.

535 **Table 3**. Enantioseparation of N-derivatized amino acids in the polar organic phase
536 mode. Experimental conditions: (a) ACN/MeOH/HAc/TEA (60/40/0.055/0.005,
537 v/v/v/v); (b) ACN/MeOH/HAc/TEA (60/40/0.11/0.01, v/v/v/v); (c)
538 ACN/MeOH/HAc/TEA (60/40/0.22/0.02, v/v/v/v). Other experimental conditions as
539 in **Figure 5**.

Figure 1.

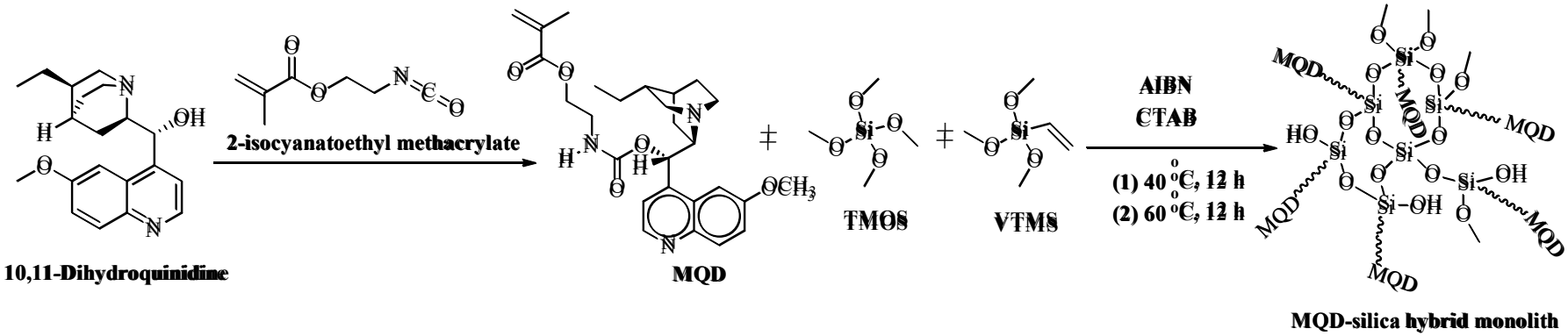
10,11-Dihydroquinidine
2-isocyanatoethyl methacrylate
MQD
TMOS
VTMS
AIBN
CTAB
(1) 40 °C, 12 h
(2) 60 °C, 12 h
MQD-silica hybrid monolith

Figure 2.

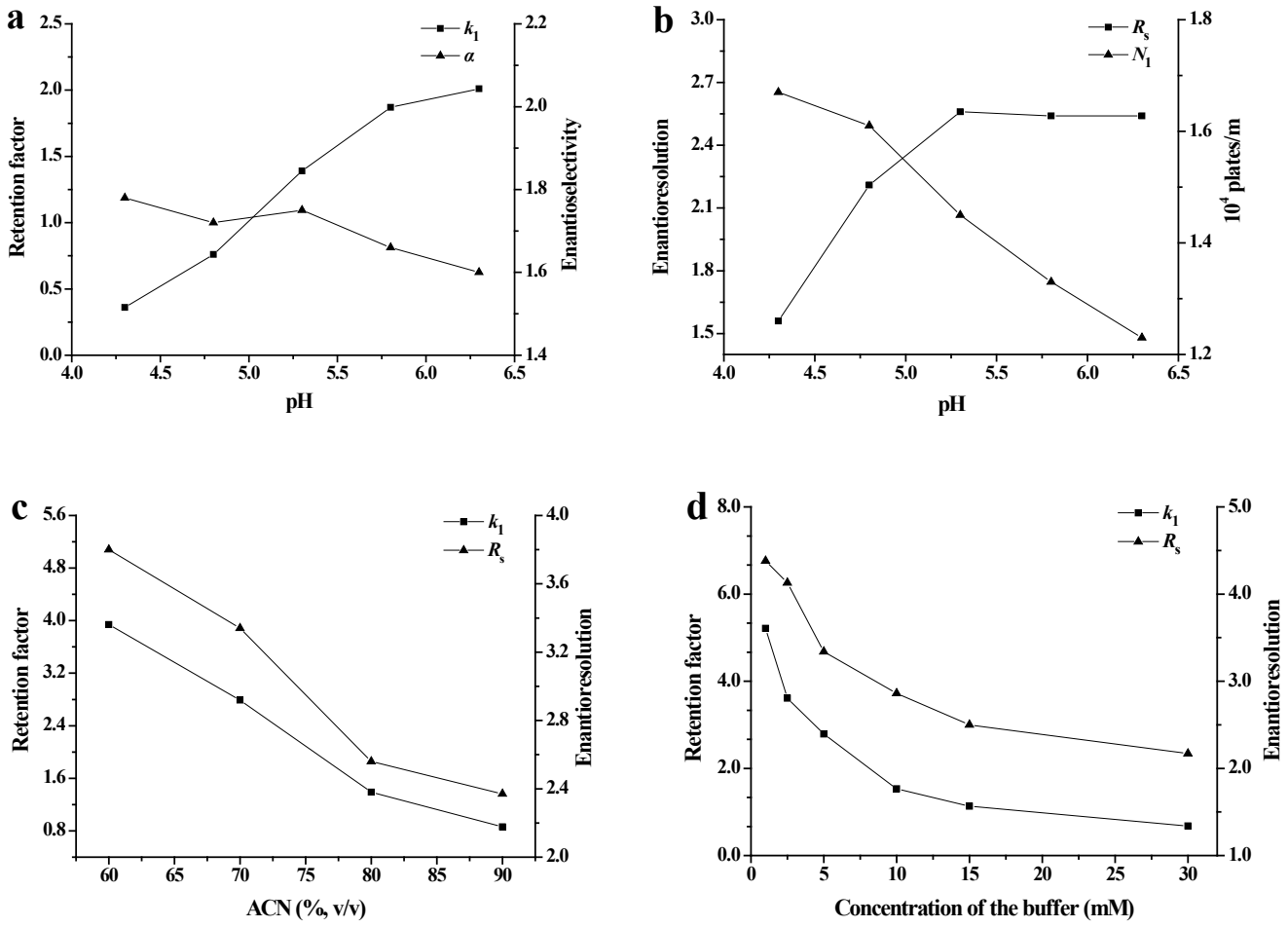
a
Retention factor
Enantioselectivity
pH
k_1
α
b
Enantioresolution
10^4 plates/m
pH
R_s
N_1
c
Retention factor
Enantioresolution
ACN (%, v/v)
k_1
R_s
d
Retention factor
Enantioresolution
Concentration of the buffer (mM)
k_1
R_s

Figure 3.

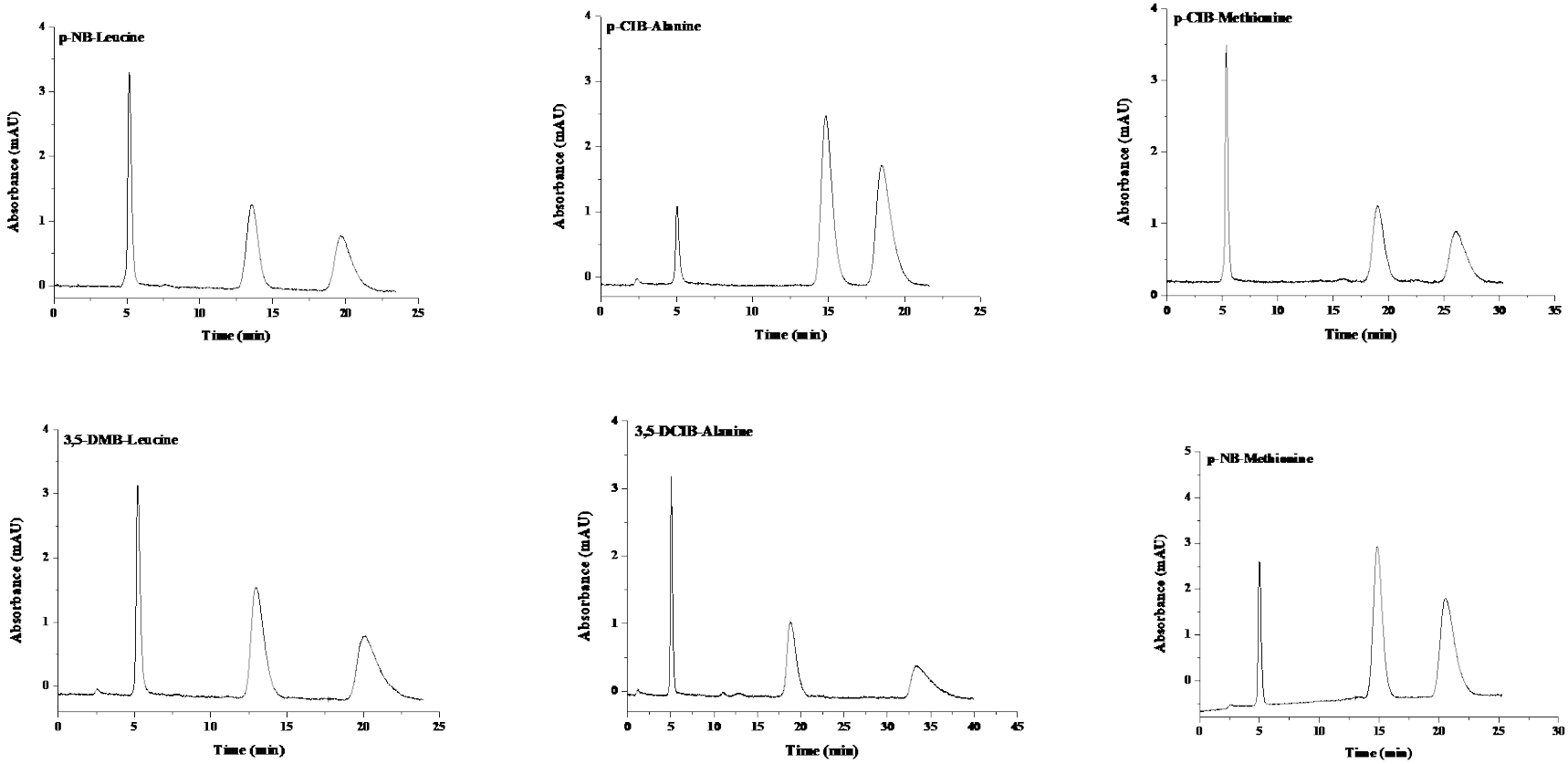
p-NB-Leucine
p-ClB-Alanine
p-ClB-Methionine
3,5-DMB-Leucine
3,5-DClB-Alanine
p-NB-Methionine
Absorbance (mAU)
Time (min)

Figure 4.

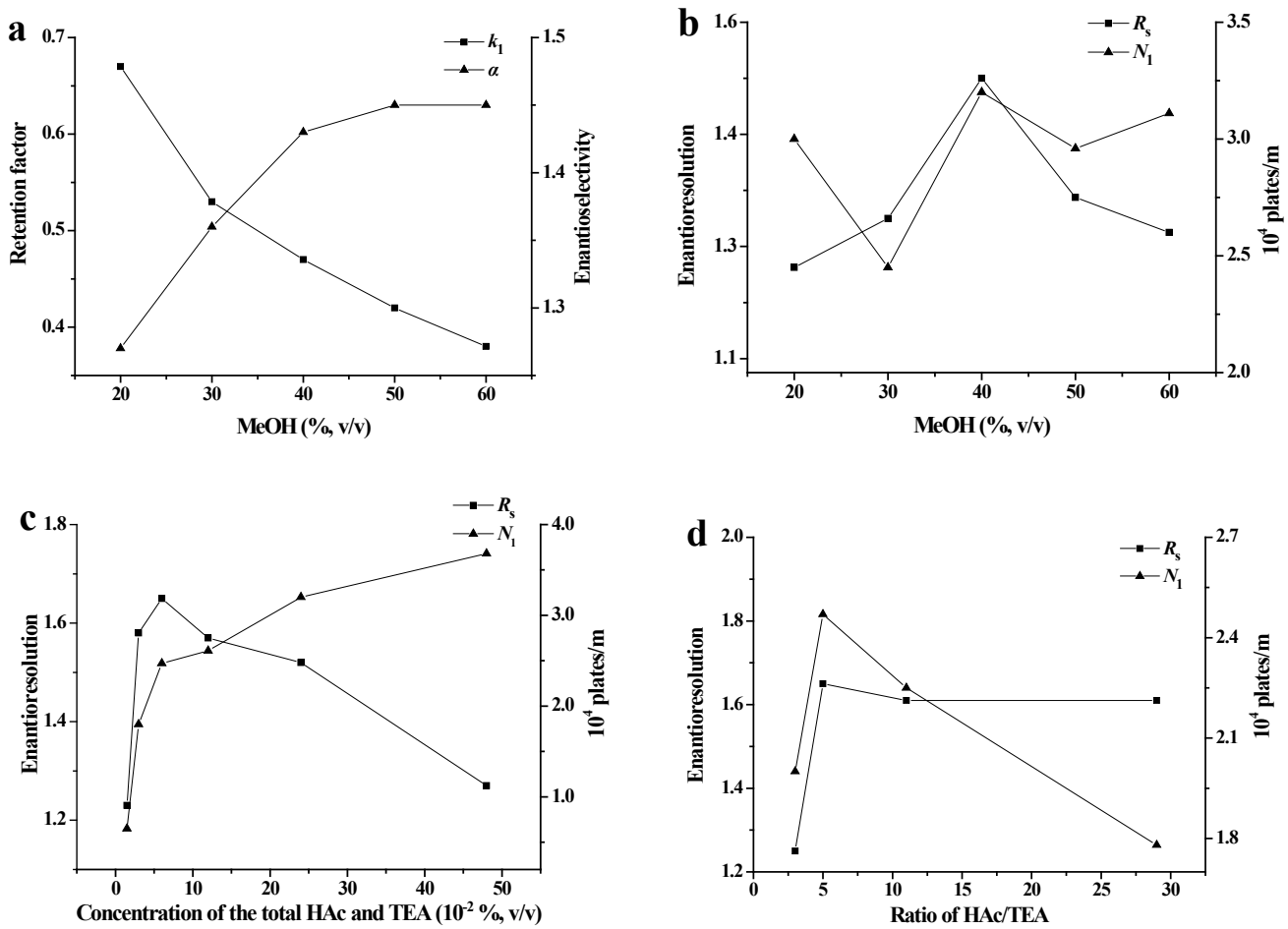
a
Retention factor
Enantioselectivity
k_1
α
MeOH (%, v/v)
b
Enantioresolution
10^4 plates/m
R_s
N_1
MeOH (%, v/v)
c
Enantioresolution
10^4 plates/m
R_s
N_1
Concentration of the total HAc and TEA (10^{-2} %, v/v)
d
Enantioresolution
10^4 plates/m
R_s
N_1
Ratio of HAc/TEA

Figure 5.

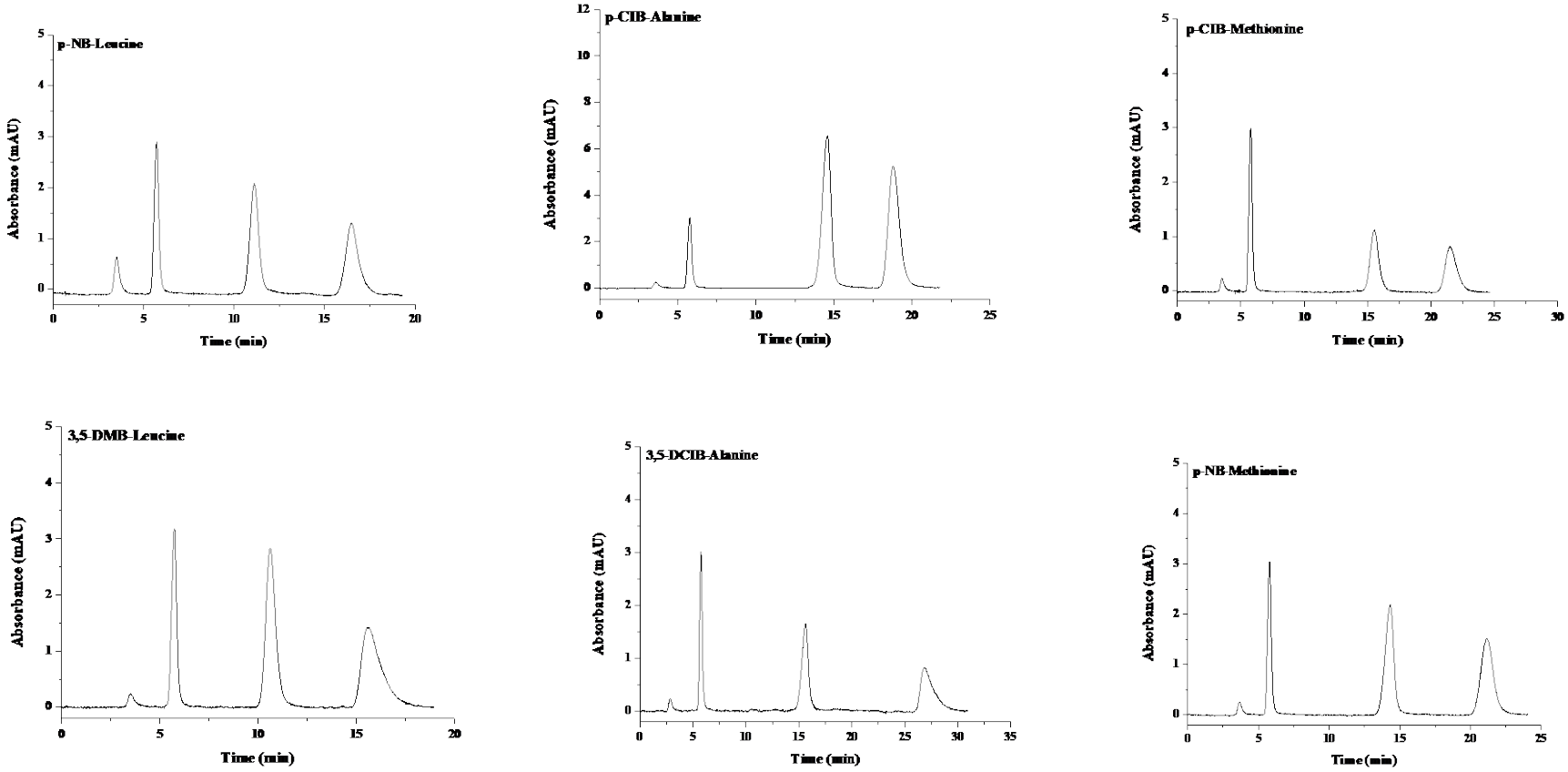
p-NB-Leucine
p-CIB-Alanine
p-CIB-Methionine
3,5-DMB-Leucine
3,5-DCIB-Alanine
p-NB-Methionine
Absorbance (mAU)
Time (min)

Figure 6.

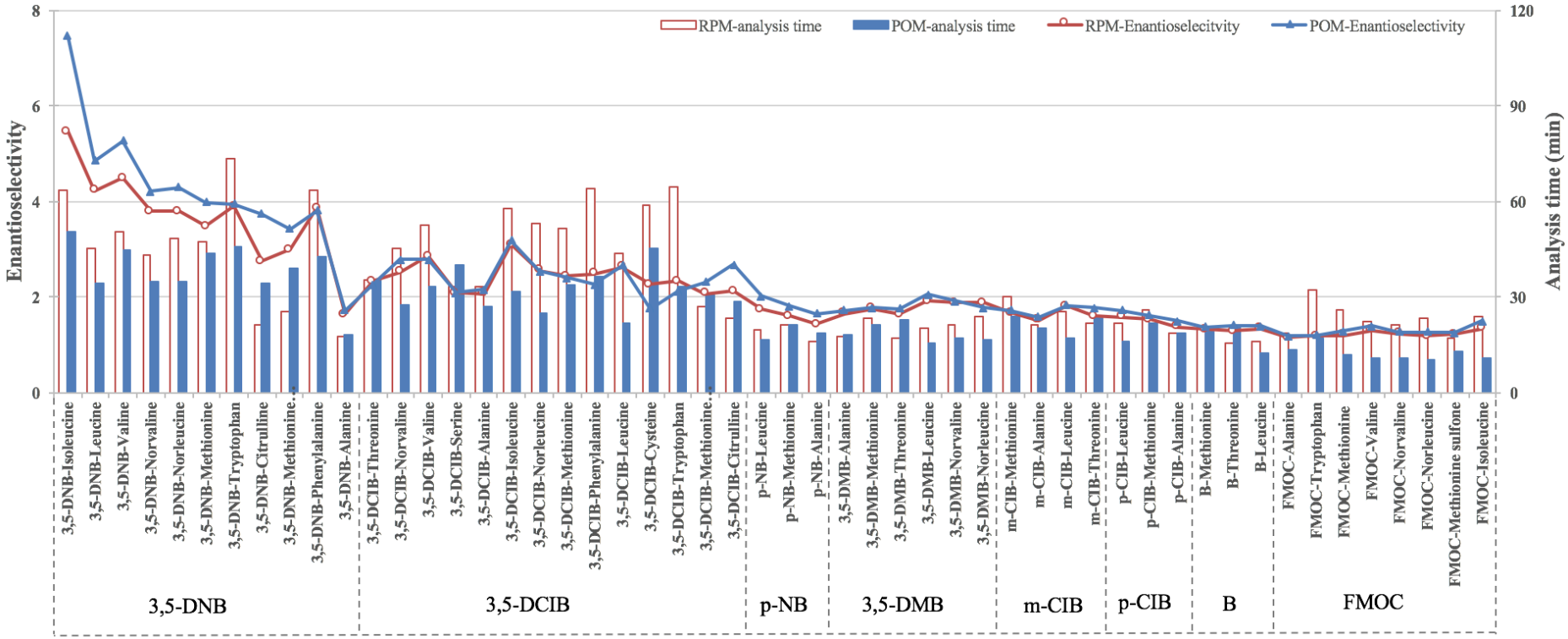
RPM-analysis time
POM-analysis time
RPM-Enantioselecitvity
POM-Enantioselectivity
Enantioselectivity
Analysis time (min)
0
2
4
6
8
0
30
60
90
120
3,5-DNB-Isoleucine
3,5-DNB-Leucine
3,5-DNB-Valine
3,5-DNB-Norvaline
3,5-DNB-Norleucine
3,5-DNB-Methionine
3,5-DNB-Tryptophan
3,5-DNB-Citrulline
3,5-DNB-Methionine...
3,5-DNB-Phenylalanine
3,5-DNB-Alanine
3,5-DCIB-Threonine
3,5-DCIB-Norvaline
3,5-DCIB-Valine
3,5-DCIB-Serine
3,5-DCIB-Alanine
3,5-DCIB-Isoleucine
3,5-DCIB-Norleucine
3,5-DCIB-Methionine
3,5-DCIB-Phenylalanine
3,5-DCIB-Leucine
3,5-DCIB-Cysteine
3,5-DCIB-Tryptophan
3,5-DCIB-Methionine...
3,5-DCIB-Citrulline
p-NB-Leucine
p-NB-Methionine
p-NB-Alanine
3,5-DMB-Alanine
3,5-DMB-Methionine
3,5-DMB-Threonine
3,5-DMB-Leucine
3,5-DMB-Norvaline
3,5-DMB-Norleucine
m-CIB-Methionine
m-CIB-Alanine
m-CIB-Leucine
m-CIB-Threonine
p-CIB-Leucine
p-CIB-Methionine
p-CIB-Alanine
B-Methionine
B-Threonine
B-Leucine
FMOC-Alanine
FMOC-Tryptophan
FMOC-Methionine
FMOC-Valine
FMOC-Norvaline
FMOC-Norleucine
FMOC-Methionine sulfone
FMOC-Isoleucine
3,5-DNB
3,5-DCIB
p-NB
3,5-DMB
m-CIB
p-CIB
B
FMOC

Figure 7.

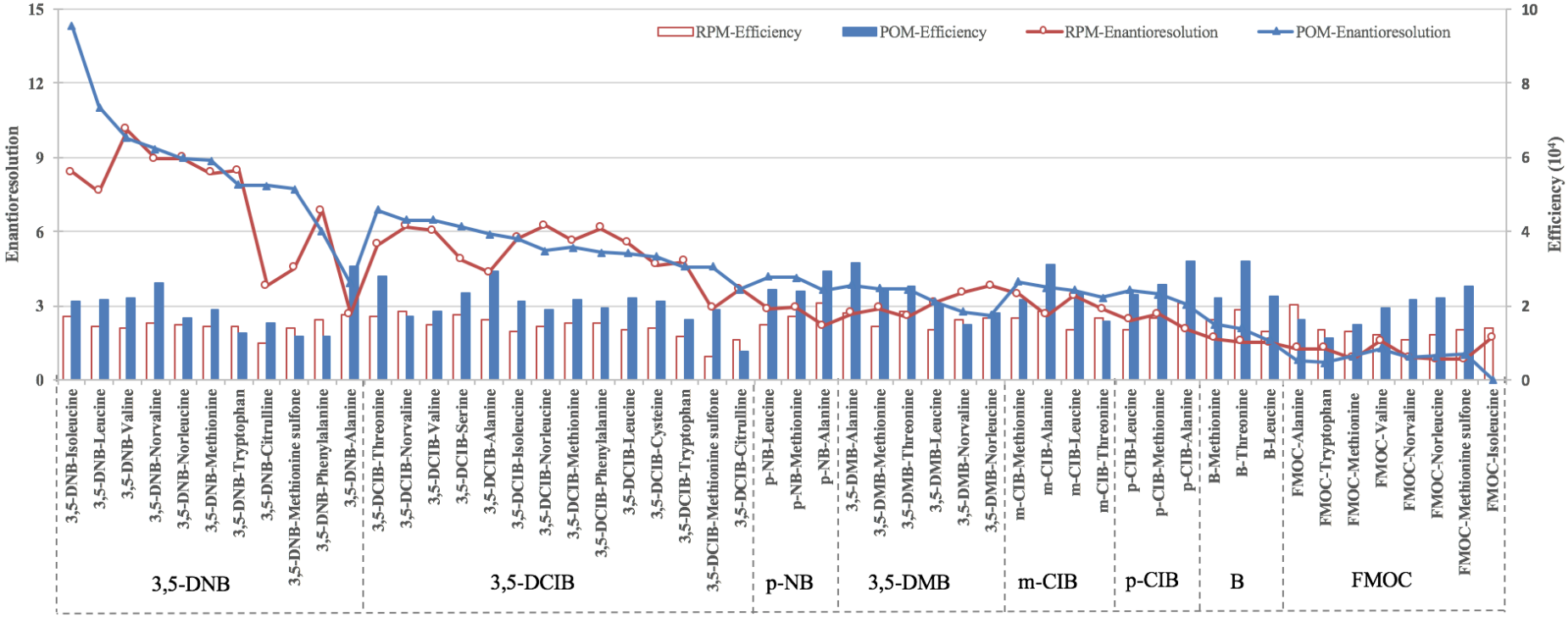
RPM-Efficiency
POM-Efficiency
RPM-Enantioresolution
POM-Enantioresolution
Enantioresolution
Efficiency (10⁴)
15
12
9
6
3
0
10
8
6
4
2
0
3,5-DNB-Isoleucine
3,5-DNB-Leucine
3,5-DNB-Valine
3,5-DNB-Norvaline
3,5-DNB-Norleucine
3,5-DNB-Methionine
3,5-DNB-Tryptophan
3,5-DNB-Citrulline
3,5-DNB-Methionine sulfone
3,5-DNB-Phenylalanine
3,5-DNB-Alanine
3,5-DCIB-Threonine
3,5-DCIB-Norvaline
3,5-DCIB-Valine
3,5-DCIB-Serine
3,5-DCIB-Alanine
3,5-DCIB-Isoleucine
3,5-DCIB-Norleucine
3,5-DCIB-Methionine
3,5-DCIB-Phenylalanine
3,5-DCIB-Leucine
3,5-DCIB-Cysteine
3,5-DCIB-Tryptophan
3,5-DCIB-Methionine sulfone
3,5-DCIB-Citrulline
p-NB-Leucine
p-NB-Methionine
p-NB-Alanine
3,5-DMB-Alanine
3,5-DMB-Methionine
3,5-DMB-Threonine
3,5-DMB-Leucine
3,5-DMB-Norvaline
3,5-DMB-Norleucine
m-CIB-Methionine
m-CIB-Alanine
m-CIB-Leucine
m-CIB-Threonine
p-CIB-Leucine
p-CIB-Methionine
p-CIB-Alanine
B-Methionine
B-Threonine
B-Leucine
FMOC-Alanine
FMOC-Tryptophan
FMOC-Methionine
FMOC-Valine
FMOC-Norvaline
FMOC-Norleucine
FMOC-Methionine sulfone
FMOC-Isoleucine
3,5-DNB
3,5-DCIB
p-NB
3,5-DMB
m-CIB
p-CIB
B
FMOC

Table 1. Effect of the preparation parameters for the MQD-silica hybrid monolithic columns.

Column	MeOH/EG (μL, v/v)	H_2O/ $NH_3 \cdot H_2O$ (μL, v/v)	CTAB (mg)	TMOS/VTMS (μL, v/v)	MQD (mg)	Temperature and Time (℃, h)	Morphology
C1	95/35	30/30	1.6	60/80	6.0	40 ℃, 12 h; 60 ℃, 12 h	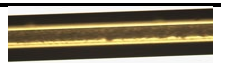
C2	100/30	30/30	1.6	60/80	6.0	40 ℃, 12 h; 60 ℃, 12 h	
C3	105/25	30/30	1.6	60/80	6.0	40 ℃, 12 h; 60 ℃, 12 h	
C4	100/30	25/30	1.6	60/80	6.0	40 ℃, 12 h; 60 ℃, 12 h	
C5	100/30	35/30	1.6	60/80	6.0	40 ℃, 12 h; 60 ℃, 12 h	
C6	100/30	30/30	1.2	60/80	6.0	40 ℃, 12 h; 60 ℃, 12 h	
C7	100/30	30/30	2.0	60/80	6.0	40 ℃, 12 h; 60 ℃, 12 h	
C8	100/30	25/30	1.6	55/85	6.0	40 ℃, 12 h; 60 ℃, 12 h	
C9	100/30	35/30	1.6	65/75	6.0	40 ℃, 12 h; 60 ℃, 12 h	
C10	100/30	30/30	1.6	60/80	4.0	40 ℃, 12 h; 60 ℃, 12 h	
C11	100/30	30/30	1.6	60/80	8.0	40 ℃, 12 h; 60 ℃, 12 h	
C12	100/30	30/30	1.6	60/80	6.0	40 ℃, 24 h	
C13	100/30	30/30	1.6	60/80	6.0	60 ℃, 24 h	

Table 2. Enantioseparation of N-derivatized amino acids in the reversed phase mode.

Sample	k_1	k_2	α	R_s	N_1 (m)	N_2 (m)
3,5-DNB-isoleucine	2.01	10.95	5.45	8.40	17300	12400
3,5-DNB-leucine	1.86	7.84	4.22	7.62	14500	11500
3,5-DNB-valine	1.85	8.31	4.49	10.10	14000	9200
3,5-DNB-norvaline	1.95	7.39	3.79	8.94	15100	10000
3,5-DNB-norleucine	2.19	8.31	3.79	8.97	14800	9500
3,5-DNB-methionine	2.24	7.80	3.48	8.37	14500	9500
3,5-DNB-tryptophan	3.30	12.83	3.89	8.47	14300	10100
3,5-DNB-citrulline	1.13	3.11	2.75	3.81	10100	7000
3,5-DNB-methionine sulfone	1.35	4.04	2.99	4.51	14000	6300
3,5-DNB-phenylalanine	2.79	10.77	3.86	6.83	16400	8700
3,5-DNB-alanine	1.50	2.45	1.63	2.65	17600	14600
3,5-DCIB-threonine	2.43	5.63	2.32	5.44	17100	15700
3,5-DCIB-norvaline	3.05	7.69	2.52	6.19	18300	13600
3,5-DCIB-valine	3.07	8.73	2.84	6.02	14700	9300
3,5-DCIB-serine	2.46	5.11	2.08	4.86	17700	16100
3,5-DCIB-alanine	2.71	5.58	2.06	4.33	16000	13500
3,5-DCIB-isoleucine	3.24	10.00	3.09	5.73	13200	9800

3,5-DCIB-norleucine	3.55	9.09	2.56	6.23	14200	11200
3,5-DCIB-methionine	3.54	8.60	2.43	5.61	15500	13800
3,5-DCIB-phenylalanine	4.43	10.99	2.48	6.13	15500	11200
3,5-DCIB-leucine	2.91	7.63	2.62	5.52	13500	10500
3,5-DCIB-cysteine	4.47	10.10	2.26	4.63	13800	9000
3,5-DCIB-tryptophan	4.66	10.86	2.33	4.78	11600	9700
3,5-DCIB-methionine sulfone	2.04	4.20	2.06	2.90	6400	5200
3,5-DCIB-citrulline	1.65	3.50	2.12	3.67	10900	8000
p-NB-leucine	1.53	2.65	1.73	2.86	15000	13600
p-NB-methionine	1.99	3.17	1.59	2.91	17000	15000
p-NB-alanine	1.50	2.14	1.43	2.17	20800	18700
3,5-DMB-alanine	1.47	2.41	1.64	2.69	18000	15700
3,5-DMB-methionine	1.91	3.35	1.75	2.87	14500	10200
3,5-DMB-threonine	1.39	2.27	1.63	2.54	18300	15000
3,5-DMB-leucine	1.37	2.62	1.91	3.11	13500	10900
3,5-DMB-norvaline	1.68	3.15	1.88	3.54	16400	14800
3,5-DMB-norleucine	1.93	3.60	1.87	3.81	16500	15000
m-CIB-methionine	2.73	4.57	1.67	3.47	16800	15200
m-CIB-alanine	2.12	3.20	1.51	2.62	18600	17600

m-CIB-leucine	2.21	3.97	1.80	3.39	13700	12200
m-CIB-threonine	1.88	3.01	1.60	2.85	16500	11000
p-CIB-leucine	2.08	3.28	1.58	2.42	13500	12800
p-CIB-methionine	2.55	3.87	1.52	2.65	16700	15000
p-CIB-alanine	1.95	2.68	1.37	2.04	20500	17600
B-methionine	2.19	2.87	1.31	1.66	16000	15500
B-threonine	1.49	1.93	1.29	1.53	19000	18200
B-leucine	1.60	2.13	1.33	1.51	13000	9500
FMOC-alanine	2.27	2.62	1.15	1.25	20300	18600
FMOC-tryptophan	4.24	5.02	1.18	1.26	13500	13000
FMOC-methionine	3.42	4.06	1.19	0.84	13200	8900
FMOC-valine	2.57	3.35	1.30	1.55	12000	9700
FMOC-norvaline	2.56	3.14	1.23	0.88	11000	8200
FMOC-norleucine	2.96	3.49	1.18	0.81	12300	9300
FMOC-methionine sulfone	1.91	2.33	1.22	0.81	13400	8500
FMOC-isoleucine	2.68	3.59	1.34	1.71	13900	8700

Experimental conditions as in **Figure 3**.

Table 3. Enantioseparation of N-derivatized amino acids in the polar organic phase mode.

Sample	k_1	k_2	α	R_s	N_1 (m)	N_2 (m)
3,5-DNB-isoleucine[a]	1.07	7.97	7.45	14.30	21100	18500
3,5-DNB-leucine[a]	1.03	5.00	4.85	11.03	21700	16900
3,5-DNB-valine[a]	1.19	6.27	5.27	9.79	22000	12300
3,5-DNB-norvaline[a]	1.16	4.87	4.20	9.35	26000	13500
3,5-DNB-norleucine[a]	1.15	4.94	4.29	8.98	16600	10000
3,5-DNB-methionine[a]	1.61	6.41	3.98	8.86	18800	13400
3,5-DNB-tryptophan[a]	1.94	7.66	3.95	7.87	12500	8950
3,5-DNB-citrulline[a]	1.28	4.79	3.74	7.84	15500	12300
3,5-DNB-methionine sulfone[a]	1.66	5.67	3.42	7.72	11700	11400
3,5-DNB-phenylalanine[a]	1.66	6.32	3.81	5.98	11600	8000
3,5-DNB-alanine[a]	1.25	2.15	1.72	3.90	30700	28300
3,5-DCIB-threonine[a]	2.28	5.13	2.25	6.87	28100	24700
3,5-DCIB-norvaline[a]	1.40	3.89	2.78	6.48	17200	16200
3,5-DCIB-valine[a]	1.65	4.59	2.78	6.47	18600	14100
3,5-DCIB-serine[a]	2.52	5.24	2.08	6.19	23400	21600
3,5-DCIB-alanine[a]	1.71	3.67	2.15	5.89	29300	26400
3,5-DCIB-isoleucine[a]	1.47	4.67	3.18	5.72	21300	9600

3,5-DCIB-norleucine[a]	1.37	3.46	2.53	5.22	18700	14900
3,5-DCIB-methionine[b]	1.52	3.64	2.39	5.34	21500	14400
3,5-DCIB-phenylalanine[a]	2.28	5.12	2.25	5.15	19500	15600
3,5-DCIB-leucine[a]	1.19	3.16	2.66	5.13	22100	13100
3,5-DCIB-cysteine[a]	4.38	7.67	1.75	4.99	21200	19000
3,5-DCIB-tryptophan[a]	2.32	4.91	2.12	4.56	16200	9200
3,5-DCIB-methionine sulfone[a]	1.95	4.50	2.31	4.56	18900	7000
3,5-DCIB-citrulline[a]	1.56	4.18	2.68	3.67	7800	2400
p-NB-leucine[a]	0.94	1.89	2.01	4.18	24300	21600
p-NB-methionine[a]	1.47	2.65	1.80	4.13	23800	21700
p-NB-alanine[a]	1.35	2.21	1.64	3.64	29300	27700
3,5-DMB-alanine[a]	1.24	2.12	1.71	3.84	31400	29200
3,5-DMB-methionine[a]	1.54	2.73	1.77	3.68	24200	18900
3,5-DMB-threonine[b]	1.24	2.18	1.76	3.67	25000	18900
3,5-DMB-leucine[a]	0.84	1.71	2.04	3.14	20400	12400
3,5-DMB-norvaline[a]	1.00	1.91	1.91	2.75	14900	10900
3,5-DMB-norleucine[a]	1.03	1.82	1.77	2.61	17900	13500
m-CIB-methionine[a]	1.78	3.06	1.72	3.96	21600	17700
m-CIB-alanine[a]	1.59	2.52	1.58	3.74	31100	28900

m-CIB-leucine[a]	1.08	1.98	1.83	3.61	23300	21800
m-CIB-threonine[c]	1.18	2.09	1.77	3.33	15700	12300
p-CIB-leucine[a]	1.01	1.74	1.72	3.63	23100	16800
p-CIB-methionine[a]	1.69	2.72	1.61	3.45	25500	23900
p-CIB-alanine[a]	1.52	2.26	1.49	3.06	31800	28300
B-methionine[a]	1.65	2.26	1.37	2.23	22000	19300
B-threonine[c]	1.06	1.48	1.40	2.08	32100	28800
B-leucine[a]	0.93	1.28	1.38	1.61	22500	17000
FMOC-alanine[a]	1.15	1.36	1.18	0.78	16200	15900
FMOC-tryptophan[a]	1.71	2.04	1.19	0.69	11100	6700
FMOC-methionine[a]	0.96	1.23	1.28	0.96	15000	8500
FMOC-valine[a]	0.70	0.97	1.39	1.26	19400	4000
FMOC-norvaline[a]	0.68	0.86	1.26	0.94	21600	16400
FMOC-norleucine[a]	0.69	0.87	1.26	0.96	22000	17500
FMOC-methionine sulfone[a]	1.13	1.42	1.25	1.01	25000	9500
FMOC-isoleucine[a]	0.66	0.99	1.50	/	/	/

Experimental conditions: (a) ACN/MeOH/HAc/TEA (60/40/0.055/0.005, v/v/v/v); (b) ACN/MeOH/HAc/TEA (60/40/0.11/0.01, v/v/v/v); (c) ACN/MeOH/HAc/TEA (60/40/0.22/0.02, v/v/v/v). Other experimental conditions as in **Figure 5**.

Supplementary information:

Figures:

Fig. S1. ESI-MS spectrum of the MQD monomer.

Fig. S2. SEM images of the MQD-silica monolithic column at different magnifications.

Fig. S3. Dependence of backpressure on linear velocity for the MQD-silica hybrid monolithic column. Experimental conditions: column dimensions: 15 cm × 100 μm I.D.; UV detection wavelength: 214 nm; injection volume: 20 nL; samples: Toluene (ACN or MeOH as mobile phase) and thiourea (ACN/H_2O (50/50, v/v) as mobile phase).

Fig. S4. Comparison of the different conditions in POM for B-threonine, *m*-CIB-threonine, 3,5-DMB-threonine and 3,5-DCIB-methionine. Experimental conditions: (a) ACN/MeOH/HAc/TEA (60/40/0.055/0.005, v/v/v/v); (b) ACN/MeOH/HAc/TEA (60/40/0.11/0.01, v/v/v/v); (c) ACN/MeOH/HAc/TEA (60/40/0.22/0.02, v/v/v/v). Column dimensions: 15 cm × 100 μm I.D.; UV detection wavelength: 254 nm; flow rate: 10 μL/min; injection volume: 20 nL.

Tables:

Table S1. Permeability of the MQD-silica hybrid monolithic column. Relative polarity and viscosity data of pure liquids were obtained from Ref. [23-24].

Table S2. Reproducibility of the MQD-silica hybrid monolith columns. Experimental conditions: column dimensions: 15 cm × 100 μm I.D.; mobile phase: ACN/10 mM ammonium acetate (70/30, v/v) (apparent pH=5.3); UV detection wavelength: 254 nm; injection volume: 20 nL; sample: *p*-NB-leucine.

Table S3. Effect of mobile phase composition on enantioseparation for 3,5-DMB-leucine under the reversed phase mode. Experimental conditions: (a) ACN/5 mM ammonium acetate (80/20, v/v) (at the desired apparent pH values); (b) ACN/5 mM ammonium acetate (at the desired ratio of ACN and buffer, v/v) (apparent pH=5.3); (c) ACN/ammonium acetate (at the desired concentration of the buffer) (70/30, v/v) (apparent pH=5.3). Column dimensions: 15 cm × 100 μm I.D.; UV detection wavelength: 254 nm; flow rate: 10 μL/min; injection volume: 20 nL.

Table S4. Effect of mobile phase composition on enantioseparation for 3,5-DCIB-leucine under the polar organic phase mode. Experimental conditions: (a)MeOH/ACN/HAc/TEA (at the desired ratio of MeOH and ACN/0.2/0.04, v/v/v/v); (b) MeOH/ACN/HAc/TEA (40/60/at the desired content of HAc and TEA, v/v/v/v); (c)

35 MeOH/ACN/HAc/TEA (40/60/at the desired ratio of HAc and TEA, v/v/v/v). Column
36 dimensions: 15 cm × 100 μm I.D.; UV detection wavelength: 254 nm; flow rate: 10
37 μL/min; injection volume: 20 nL.

Figure S1.

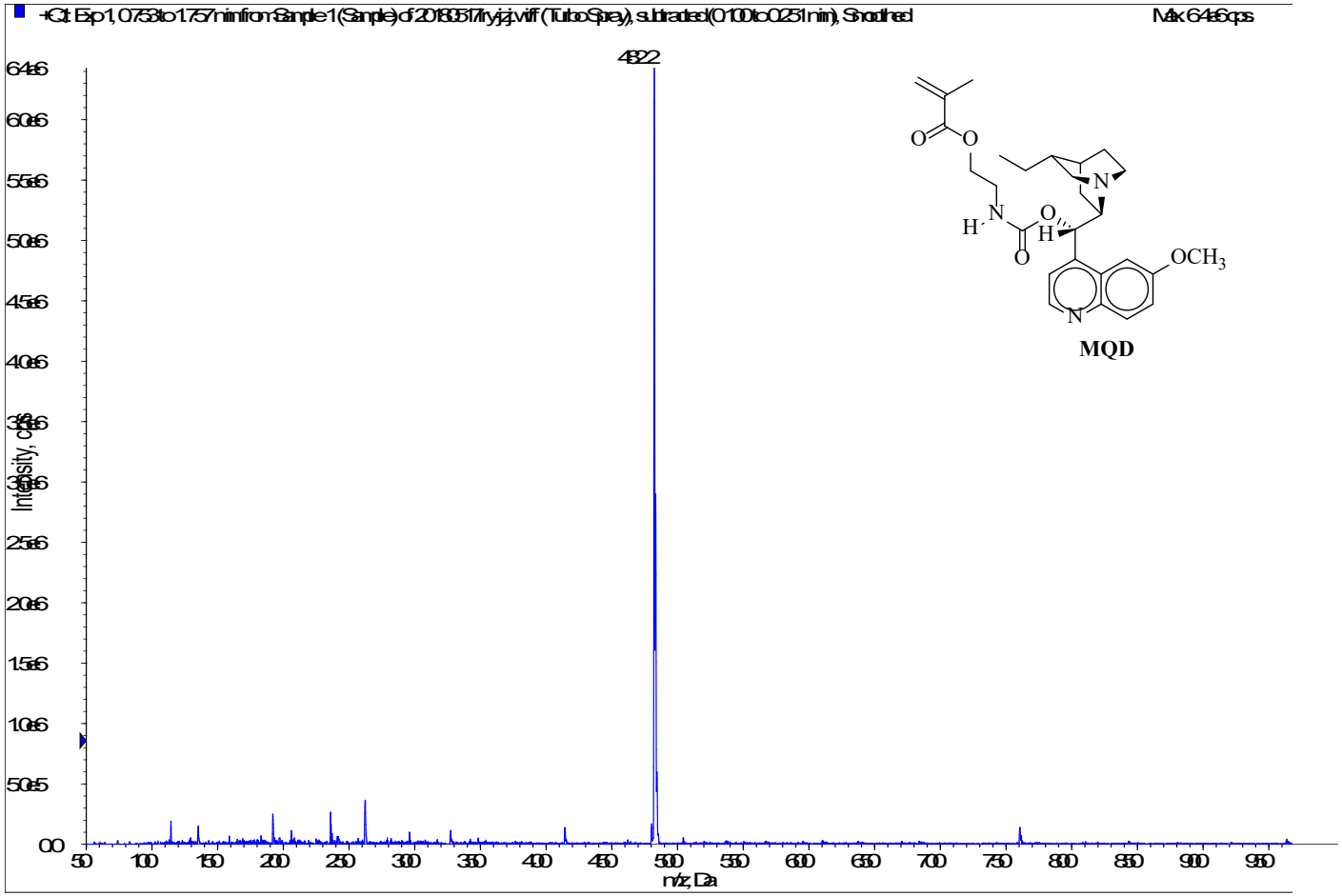
+Q1: Exp 1, 0.753 to 1.757 min from Sample 1 (Sample) of 20130317ryjz.wiff (Turbo Spray), subtracted (0.100 to 0.251 min), Smoothed
Max. 6.4e6 cps.
482.2
Intensity, cps
m/z, Da
MQD

Figure S2.

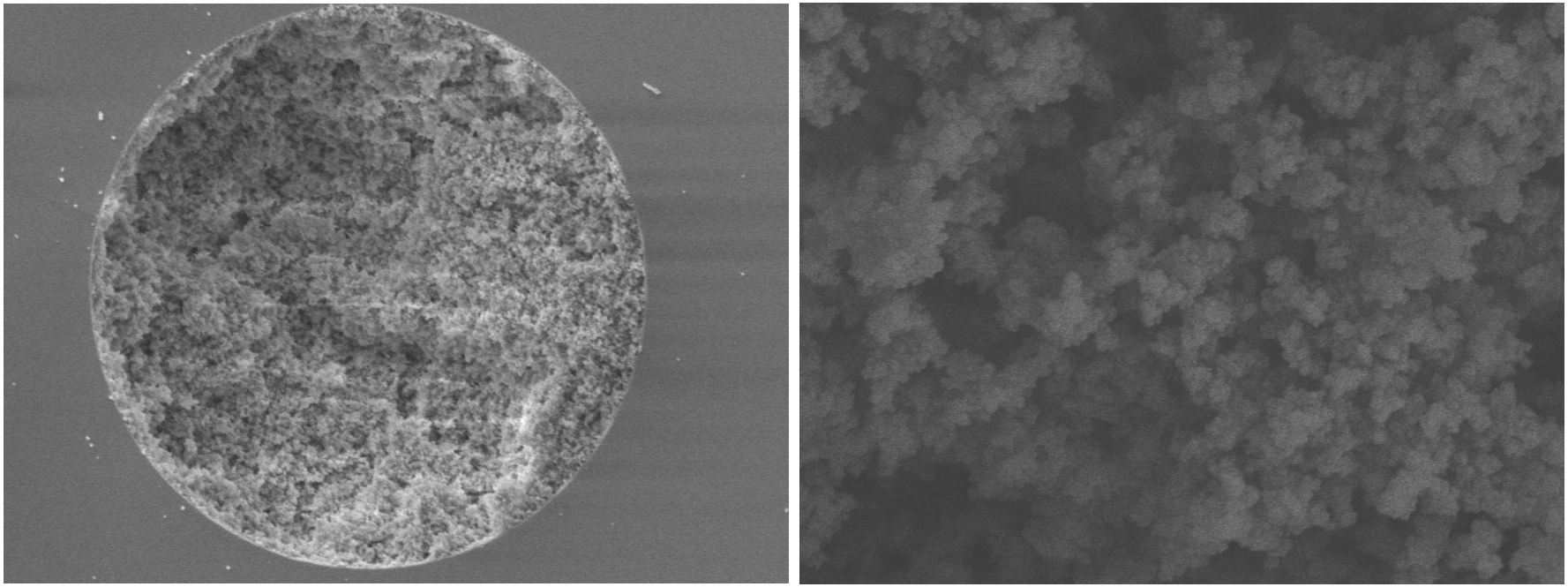

51 **Figure S3.**

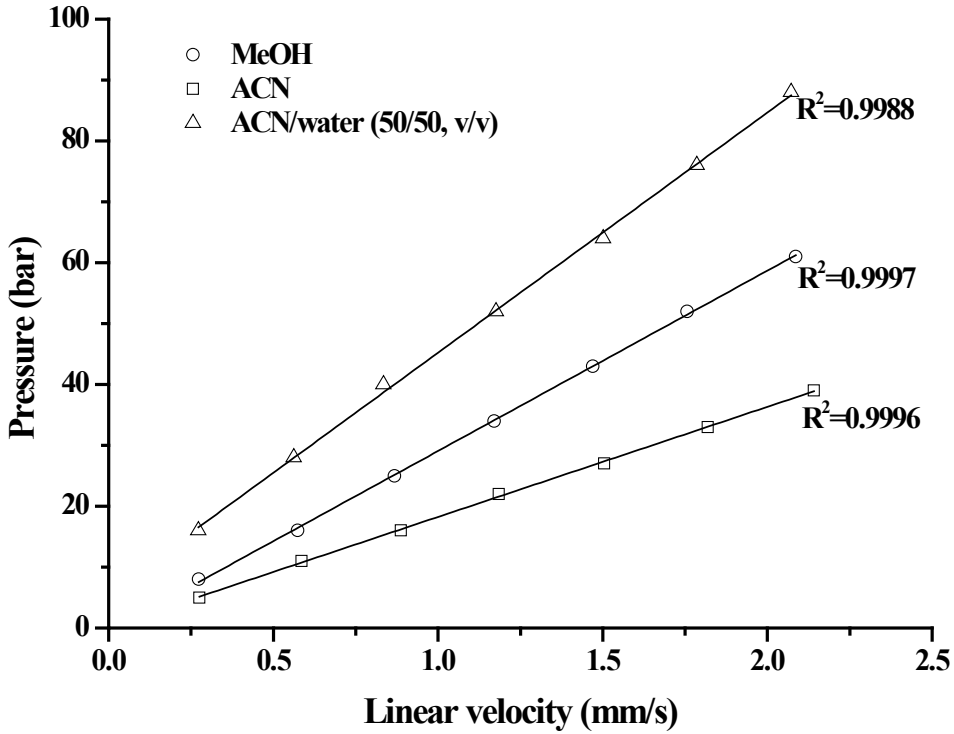

52

53

54 **Figure S4.**

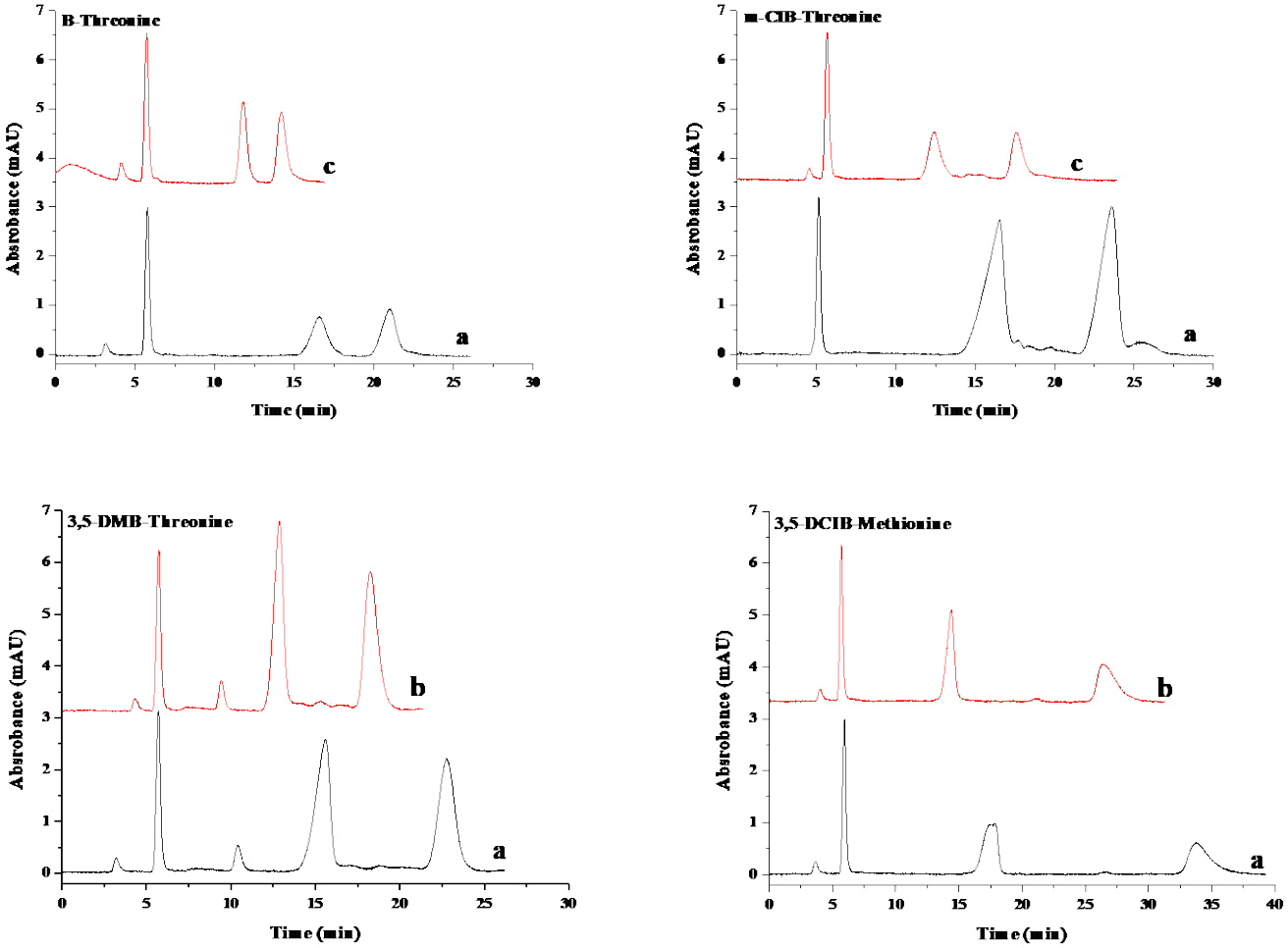

55

56

Table S1. Permeability of the MQD-silica hybrid monolithic column.

Mobile phase	Relative polarity	Viscosity η ($\times 10^{-3}$ Pa·s)	Permeability K ($\times 10^{-14}$ m^2)
ACN	0.460	0.369	2.95
MeOH	0.762	0.544	2.93
ACN/H_2O (50:50, v/v)	/	0.820	2.47

Relative polarity and viscosity data of pure liquids were obtained from Ref. [23,24].

66 **Table S2.** Reproducibility of the MQD-silica hybrid monolith column.

	Average retention factor (RSD)		Average selectivity α (RSD)	Average resolution R_s (RSD)
	k_1	k_2		
Run to run (n=6)	1.51 (1.81%)	2.63 (1.24%)	1.74 (1.64%)	2.83 (2.07%)
Column to column (n=5)	1.54 (2.53%)	2.64 (3.05%)	1.72 (3.04%)	2.85 (3.90%)
Batch to batch (n=3)	1.52 (4.29%)	2.66 (3.59%)	1.76 (4.04%)	2.84 (2.88%)
Day to day (n=3)	1.53 (1.73%)	2.67 (1.69%)	1.75 (1.10%)	2.85 (1.07%)

67 Experimental conditions: column dimensions: 15 cm × 100 μm I.D.; mobile phase: ACN/10 mM ammonium acetate (70/30, v/v) (apparent pH=5.3); UV detection
68 wavelength: 254 nm; injection volume: 20 nL; sample: p-NB-leucine.

Table S3. Effect of mobile phase composition on enantioseparation for 3,5-DMB-leucine under the reversed phase mode

	Sample	k_1	k_2	α	R_s	N_1 (m)	N_2 (m)
Effect of the apparent pH[a]							
pH=4.3	3,5-DMB-leucine	0.29	0.54	1.86	1.51	14700	12200
pH=4.8	3,5-DMB-leucine	0.59	1.15	1.95	2.12	13000	9870
pH=5.3	3,5-DMB-leucine	1.19	2.32	1.95	2.71	12050	8570
pH=5.8	3,5-DMB-leucine	1.79	3.40	1.90	2.77	9300	8200
pH=6.3	3,5-DMB-leucine	1.88	3.31	1.76	2.66	9050	8700
Effect of ACN content[b]							
60%	3,5-DMB-leucine	3.76	7.30	1.94	3.98	12400	10800
70%	3,5-DMB-leucine	2.36	4.59	1.94	3.40	12000	9000
80%	3,5-DMB-leucine	1.19	2.32	1.95	2.71	12050	8570
90%	3,5-DMB-leucine	0.70	1.32	1.89	2.58	14000	12700
Effect of the buffer concentration[c]							
1 mM	3,5-DMB-leucine	5.14	9.97	1.94	4.02	12000	9900
2.5 mM	3,5-DMB-leucine	3.05	5.95	1.95	3.92	12300	11300
5.0 mM	3,5-DMB-leucine	2.36	4.59	1.94	3.40	12000	9000
10.0 mM	3,5-DMB-leucine	1.37	2.62	1.91	3.11	13500	10900
15.0 mM	3,5-DMB-leucine	0.97	1.98	2.04	2.87	12400	10200
30.0 mM	3,5-DMB-leucine	0.63	1.25	1.98	2.39	13900	11400

Experimental conditions: (a) ACN/5 mM ammonium acetate (80/20, v/v) (at the desired apparent pH values); (b) ACN/5 mM ammonium acetate (at the desired ratio of ACN and buffer, v/v) (apparent pH=5.3); (c) ACN/ammonium acetate (at the desired concentration of the buffer) (70/30, v/v) (apparent pH=5.3). Column dimensions: 15 cm × 100 μm I.D.; UV detection wavelength: 254 nm; flow rate: 10 μL/min; injection volume: 20 nL.

93 **Table S4.** Effect of mobile phase composition on enantioseparation for 3,5-DCIB-leucine under the polar organic phase mode.

	Sample	k_1	k_2	α	R_s	N_1 (m)	N_2 (m)
Effect of the volume ratio of MeOH/ACN[a]							
60:40 (v/v)	3,5-DCIB-leucine	0.45	1.33	2.96	4.09	26500	13600
50:50 (v/v)	3,5-DCIB-leucine	0.49	1.46	2.98	4.30	25800	14000
40:60 (v/v)	3,5-DCIB-leucine	0.50	1.47	2.94	4.29	24100	14200
30:70 (v/v)	3,5-DCIB-leucine	0.58	1.56	2.69	3.91	25400	11500
20:80 (v/v)	3,5-DCIB-leucine	0.72	1.71	2.38	3.85	30100	12700
Effect of the HAc+TEA total content (v/v)[b]							
0.015 % (0.0125% HAc +0.0025% TEA)	3,5-DCIB-leucine	1.36	3.23	2.38	4.38	8200	18400
0.03% (0.025% HAc + 0.005% TEA)	3,5-DCIB-leucine	1.02	2.57	2.52	4.42	13900	14100
0.06% (0.05% HAc + 0.01% TEA)	3,5-DCIB-leucine	0.87	2.26	2.60	4.51	20000	13200
0.12% (0.1% HAc + 0.02% TEA)	3,5-DCIB-leucine	0.67	1.79	2.67	4.37	23000	13800
0.24% (0.2% HAc + 0.04% TEA)	3,5-DCIB-leucine	0.50	1.47	2.94	4.29	24100	14200
0.48% (0.4% HAc + 0.08% TEA)	3,5-DCIB-leucine	0.36	1.03	2.86	3.92	34100	17100
Effect of the ratio of HAc/TEA[c]							
3:1 (v/v)	3,5-DCIB-leucine	0.67	1.69	2.52	4.24	18600	17800
5:1 (v/v)	3,5-DCIB-leucine	0.87	2.26	2.60	4.51	20000	13200
11:1 (v/v)	3,5-DCIB-leucine	1.19	3.16	2.66	5.13	22100	13100

29:1 (v/v)	3,5-DCIB-leucine	1.43	3.86	2.70	5.12	22900	1100094

Experimental conditions: (a)MeOH/ACN/HAc/TEA (at the desired ratio of MeOH and ACN/0.2/0.04, v/v/v/v); (b) MeOH/ACN/HAc/TEA (40/60/at the desired content of HAc and TEA, v/v/v/v); (c) MeOH/ACN/HAc/TEA (40/60/at the desired ratio of HAc and TEA, v/v/v/v). Column dimensions: 15 cm × 100 μm I.D.; UV detection wavelength: 254 nm; flow rate: 10 μL/min; injection volume: 20 nL.